ICAS-82-4.4.5

THE PREDICTION OF PROPELLER/WING INTERACTION EFFECTS

Abdullah S. Aljabri
Lockheed-Georgia Company
Marietta, Georgia

Abstract

An analytical technique has been developed which predicts the influence of a propeller slipstream on a nacelle/wing combination. This is achieved by coupling a slipstream code with a complex configuration potential flow analysis code. The slipstream code is based on the vortex theory of propellers and predicts the slipstream in terms of its shape induced velocities and swirl angle. To verify the slipstream code two experiments with different model propellers were carried out. The wake immediately behind these propellers was surveyed and results compared with predictions. Good correlation is obtained. The coupling of the slipstream code with the panel code allows analysis of propeller slipstream/nacelle/wing combinations. Results comparing the wing spanwise loading with and without slipstream are presented. The computational results are found to be in good agreement with experimental data.

Nomenclature

a	Airfoil lift curve slope
B	Number of propeller blades
c	Blade chord
c_d	Airfoil Section drag coefficient
c_l	Airfoil section lift coefficient
c_{l_i}	Airfoil section design lift coefficient
C_P	Power coefficient
C_T	Thrust coefficient
D	Propeller diameter
F	Prandtl's tip loss factor
J	Advance ratio
n	Propeller rotational frequency in revolutions per second
P	Power
T	Torque
R	Propeller radius
R'	Radius of contracted wake
r	Radial distance to blade element
T	Thrust
V_o	Free stream velocity
V_e	Effective resultant velocity, Figure 1
V_R	Resultant velocity, Figure 1
V_T	Blade tip velocity
W	Velocity in the Z direction
w_a	Axial component of induced velocity
w_t	Tangential component of induced velocity
w	Induced velocity
x	Fraction of tip radius
z	Axial position downstream
α	Angle of attack
α_i	Induced angle of attack
α_t	Propeller thrust axis angle of attack
Γ	Circulation as a function of r
β	Geometric pitch angle of zero lift line
Δ	Small quantity or change
ϵ	Swirl angle
η	Propeller efficiency
κ	Goldstein's Kappa Factor
ρ	Mass density of air
ϕ	Angle formed by V_R and horizontal plane, Figure 1
ψ	Blade azimuth angle
ω	Propeller rotational frequency in radians per second

Introduction

The dramatic reduction in fuel consumption which is predicted for the propfan propulsion system has stimulated interest in high subsonic speed turboprop airplanes (Reference 1). One feasible configuration would employ a swept back wing of high aspect ratio and tractor mounted propfans. The aerodynamic effects of the slipstream from these highly loaded propellers on the performance of the wing are a major concern and have to be determined. A nacelle/wing combination which is poorly matched to the propeller slipstream can be inefficient and subject to excessive installation losses. The study of propeller slipstream/wing interaction described here is divided into two parts. The first part deals with the slipstream produced by a given propeller. Here, a computer

code is described for calculating the slipstream shape, the induced velocities, and the spanwise and downstream variation of these velocities. The second part treats the behavior of a wing in a propeller slipstream. Here the slipstream code is coupled with a potential flow analysis code to allow the influence of the slipstream on wing performance to be predicted.

Method for Predicting Propeller Slipstream

The aim of any propeller analysis is to determine the velocities induced by the helical vortex system behind the propeller. Once the induced velocities are found, both the loads on the blades and the properties of the slipstream can be determined. Consider the velocity diagram of a propeller blade section as pictured in Figure 1. The section is being influenced by the following components: the free stream velocity, V_o; the linear velocity due to blade rotation, ωr; and the induced velocity w. The current trend is to calculate the induced velocity, w, by the application of the Biot-Savart law on the helical trailing vortex system. Usually an assumption regarding the shape of the wake is made, that is, the so called prescribed wake analysis. Alternatively, a free-wake analysis can be carried out, where the location of the trailing vortex system is determined by mutual interaction between it and its induced velocities. These methods may require excessive computation time which in the free-wake case may be prohibitive, the approach developed in this paper which is based on Goldstein's propeller analysis is more efficient with regard to computer time and storage space.

The method employed here incorporates corrections for profile drag, finite section thickness and finite chord. This method predicts propeller thrust and power in close agreement with experimental measurements over a wide range of propeller geometries and operating conditions. The details of this method can be found in Reference 2 and 3, and are not repeated here.

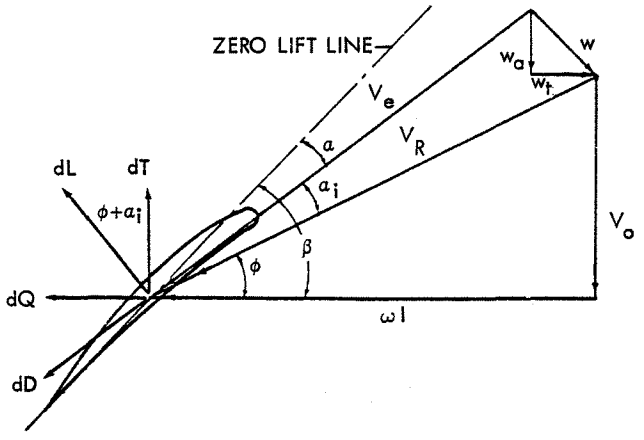

Figure 1. Velocity Diagram on Blade Section Looking Toward the Hub

Calculations Within the Slipstream

The wake behind the propeller is assumed to be axisymmetric and undistorted. The tangential induced velocity behind the propeller for an uncontracted wake remains constant with axial distance and is given by $2Kw_t(r)$. On the other hand, the axial induced velocity $w_a(r)$ increases continually through the disc plane. It increases from a value of zero infinitely far ahead of the propeller plane to a maximum value of $2w_a$ infinitely far behind the propeller.

An approximation for the axial variation can be found by calculating the axial induced velocity along the axis of a semi-infinite helical vortex filament. Using this approach, the axial induced velocity is given in terms of the velocity at the propeller plane by the following expression

$$\frac{w_a(z)}{w_a(o)} = 1 + \frac{Z/R}{\sqrt{1+(Z/R)^2}} \qquad (1)$$

where R is the propeller radius, z is the position downstream from the propeller disk, $w_a(z)$ is the induced axial velcoity at z, and $w_a(o)$ is the induced axial velocity at the propeller plane.

The swirl angle, at any position behind the disk is then given by

$$\epsilon(r,z) = \tan^{-1}\frac{2\varkappa w_t(r)}{V_o+\varkappa w_a(r,z)} \qquad (2)$$

Slipstream Contraction

To account for contraction, the continuity criterion is applied to the slipstream. From continuity

$$\rho\pi R^2(o)\,[V_o+\varkappa w_a(0)] = \rho\pi R^2(Z)\,[V_o+\varkappa w_a(Z)] \qquad (3)$$

This becomes

$$R(Z)/R(0) = [V_o+\varkappa w_a(0)]/[V_o+\varkappa w_a(Z)] \qquad (4)$$

R (z) gives the radius of the slipstream and thus the locus of R (z) gives the shape of the slipstream boundary. Figure 2 shows the shape of the slipstream and the variation of the axial induced velocity.

The tangential induced velocity is affected by this contraction. Conservation of circulation gives

$$4\pi\varkappa k\,w_t(0)/B = 4\pi r(z)\,\varkappa(z)\,w_t(Z)/B \qquad (5)$$

or

$$w_t(z) = [\varkappa r w_t(0)] / [\varkappa(z) r(z)] \qquad (6)$$

The swirl angle behind the propeller is now found from equation (1).

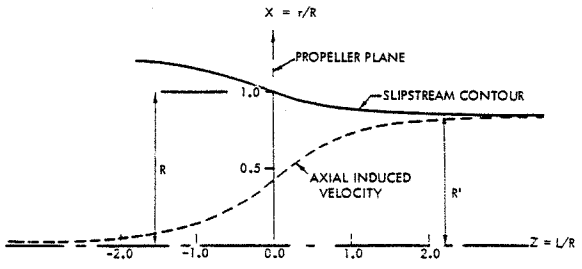

Figure 2. Characteristics of a Propeller Slipstream

Propeller At An Angle Of Attack

A qualitative approach is presented here to provide some insight to the problem of a propeller at an angle of attack. Figure 3a shows a side view of a propeller disk with the thrust axis inclined at α_t to the free stream velocity V_o. The free stream velocity can be resolved into a component $V_o \cos\alpha_t$, normal to the plane of rotation, and a component $V_o \sin\alpha_t$ parallel to the plane of rotation. Figure 3b shows a view perpendicular to the propeller plane.

A blade section operates with an equivalent free stream velocity of magnitude $V_o \cos\alpha_t$ and a rotational component $r + V_o \sin\alpha_t \sin\psi$, constant in direction but varying in magnitude with azimuthal position. Consequently, the blade can be considered to operate at a varying advance ratio. This variation is sinusoidal and reaches a maximum along $\psi = 270^\circ$ and a minimum along $\psi = 90^\circ$.

It has been determined in Reference 4 that this instantaneous advance ratio is given by:

$$J(\psi) = \frac{\pi x J \cos\alpha_t}{\pi x + J \sin\alpha_t} \qquad (7)$$

from which the maximum increment in advance ratio ΔJ is found to be:

$$\Delta J/J = \frac{J \sin\alpha_t + \pi x - \pi x \cos\alpha_t}{\pi x + J \sin\alpha_t} \qquad (8)$$

For small angles of attack Equation (8) reduces to

$$\frac{\Delta J}{J} = \frac{J \sin\alpha_t}{\pi x + J \sin\alpha_t} \qquad (9)$$

Consider a propeller operating at an advance ratio of 1.4 and an angle of attack of 5°. The maximum percentage increment in advance ratio is found to be 4% to 9% depending on the radial position. This gives rise to a 3% to 8% change in swirl angles.

Because the axial induced velocity by a propeller is always normal to the propeller plane, the flow through a propeller at an angle of attack is turned downward. Thus when a probe surveying the wake is positioned parallel to the free stream, it will sense a downward velocity of magnitude $w_a \sin\alpha_t$. This will contribute an additional increment to the swirl angle, $\Delta\epsilon$. $\Delta\epsilon$ will also vary sinusoidaly and its value is given by

$$\Delta\epsilon = \tan^{-1} \frac{w_a \sin\alpha_t \sin\psi}{V_o + w_a} \qquad (10)$$

The computer program which accomplishes the foregoing is described in Reference 2. The input to this program is a geometric description of the propeller and its operating conditions. The code defines the undisturbed slipstream by its boundary shape and by the radial distributions of its local vorticity, induced velocity and swirl angle.

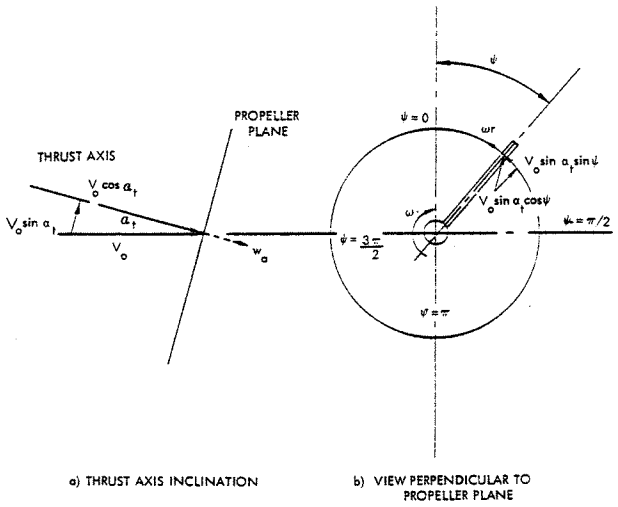

Figure 3. Propeller at Angle of Attack

Correlation of Experiment with Theory

This section presents the finding of two experiments that were carried out on model propellers.

The first was a test in the Lockheed-California subsonic wind tunnel of a four-bladed 11.2-inch diameter model propeller. The blades have 16-series airfoil sections and the propeller was driven by an electric motor housed in a nacelle. Wake surveys were made 1 inch aft of the propeller plane with a 7-probe, 5-holes-per-probe survey rake.

Comparisons between wake survey test data and theoretical results are shown in Figures 4 and 5 for an advance ratio of 0.78. All three wake parameters; axial induced velocity, tangential induced velocity, and swirl angle, show close agreement outboard. The differences inboard are probably because the theory makes no correction for nacelle-induced velocities.

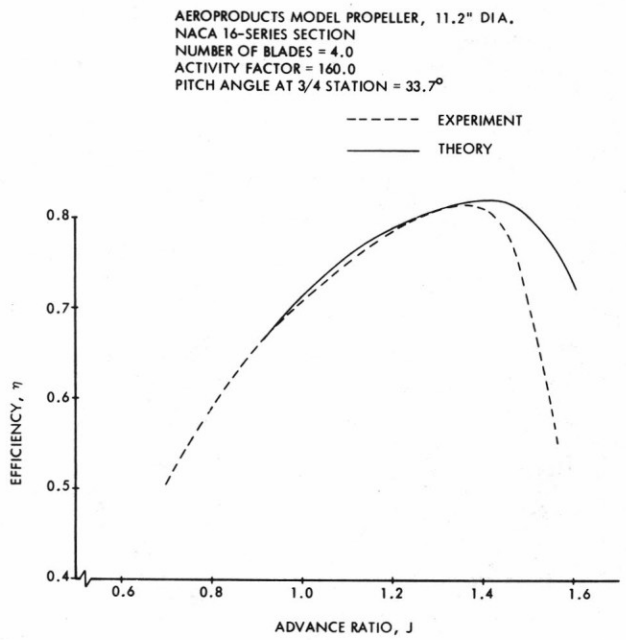

Figure 4. Comparison of Calculated and Measured Propeller Efficiency

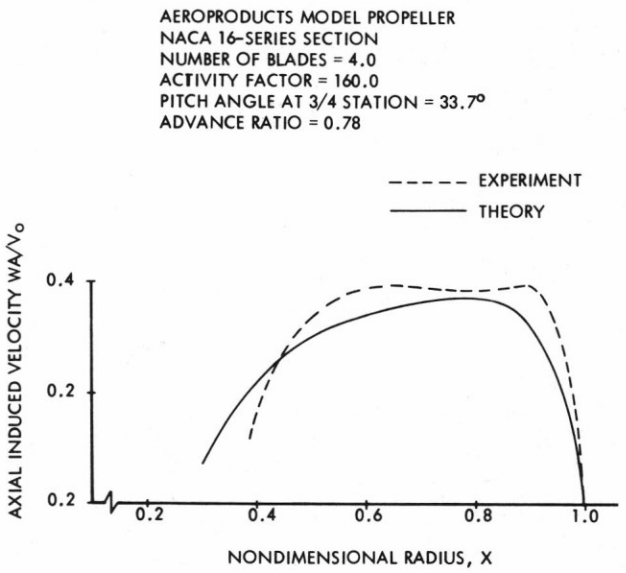

Figure 5a. Comparison of Calculated and Measured Axial Induced Velocity Distribution

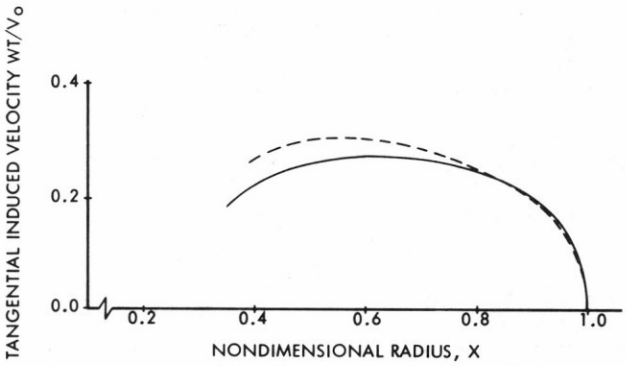

Figure 5b. Comparison of Calculated and Measured Tangential Induced Velocity Distribution

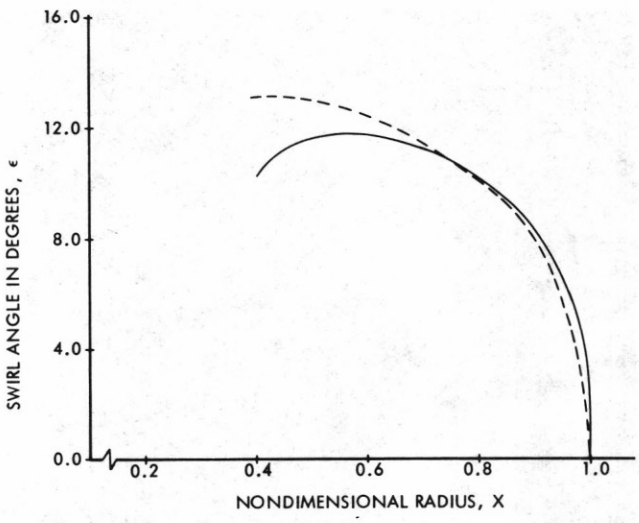

Figure 5c. Comparison of Calculated and Measured Swirl Angle Distribution

Anechoic Wind Tunnel Used to Obtain Further Correlation with Theory

The second experiment was a test of a C-130 model propeller in the Lockheed-Georgia Anechoic Wind Tunnel. A 1/10-scale C-130 propeller complete with a 1/10-scale C-130 wing and nacelle was employed (Figures 6a and 6b). Provision was made to run the propeller/nacelle on its own without the wing. No force data were taken in this test, but the propeller wake was surveyed by the same 7-probe rake used in the previously discussed test.

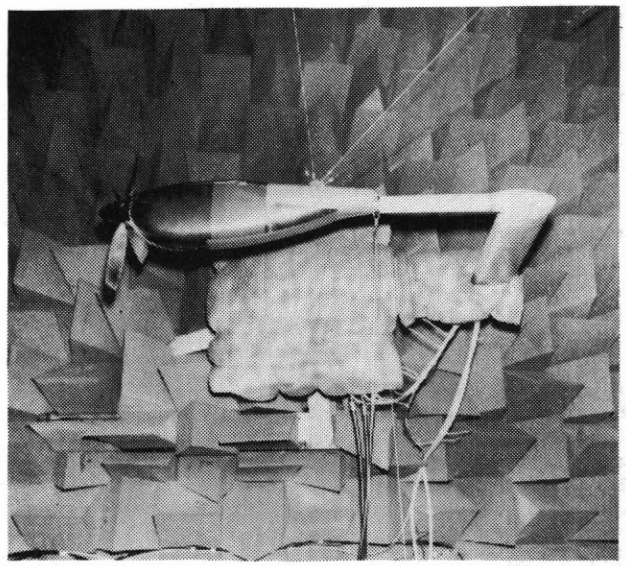

Figure 6a. C-130 1/10 Scale Model Propeller, Nacelle and Wing in Anechoic Wind Tunnel

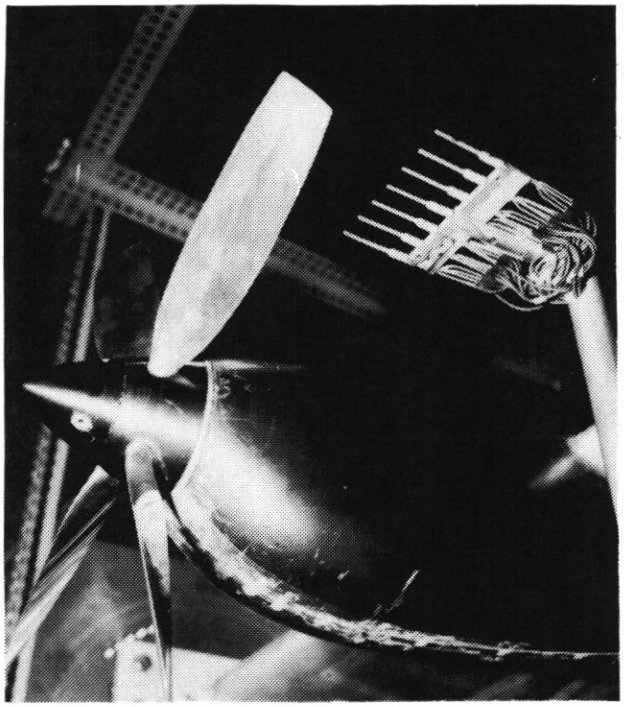

Figure 6b. The Seven Probe Rake in Position behind the Propeller Plane

Wake Surveys Yield Valuable Insight into Flow Field Characteristics

The test data were reduced to give the three components of the wake velocity, U, V, and W, from which the circulation, kinetic energy, and total pressure within the wake are computed. Maps of these aerodynamic parameters were made to give a visual demonstration of the nature of the propeller wake. Figures 7 and 8 are the results for a propeller/nacelle/wing combination at an advance ratio of 1.0 and zero angle of attack. Figure 7 is a contour map of lines of constant axial velocity with radius. Movement from one contour to an adjacent one represents an incremental change in the magnitude of axial velocity ($0.04 \times V_o$). Closely spaced lines indicate a region of rapid change while sparsely spaced lines indicate one of slow change. This change becomes rapid in approaching the blade tip, for the velocity gradually increases from the hub to reach a maximum value between the 0.8 and 0.95 radial station, after which it drops to zero in a small distance. The distribution of axial velocity is a reflection of the blade loading.

Figure 8 is a V-W vector map, presenting the V and W components of crossflow. The straight lines represent the vectorial sum of the tangential and radial velcoities, with their length indicating the magnitude of the vector at that point. Clearly the tangential velocity, which represents swirl in the slipstream, is dominating. The radial velocity is generally weak, and its contribution is appreciable only close to the nacelle surface. This vector map vividly marks the boundary of the slipstream, within which the flow is swirling and outside has no swirl. The swirl angles on the right side of the horizontal axis ($\psi = 90^o$) are noticeably less than those on the left ($\psi = 270^o$) due to an upwash field that the slipstream is experiencing, and due to interference from the nacelle, which is not axisymmetric in shape. This effectively induces an additional upwash field.

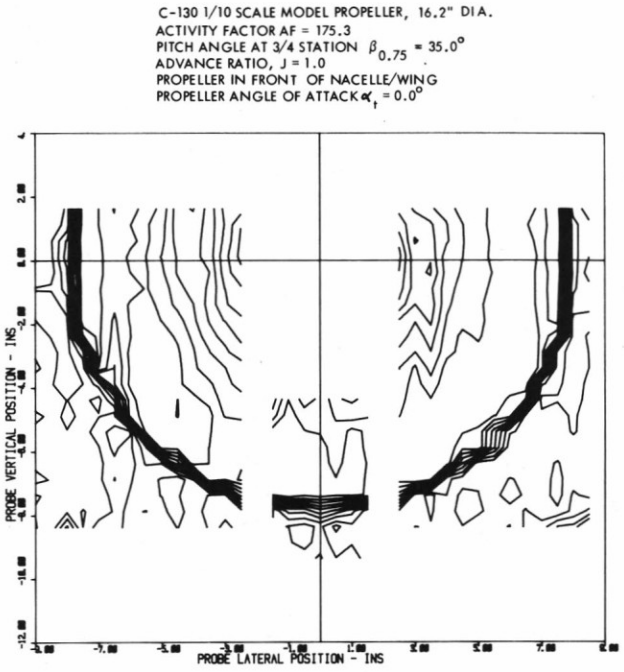

Figure 7. Axial Velocity Map of Wake (Lines of Constant U/V_o)

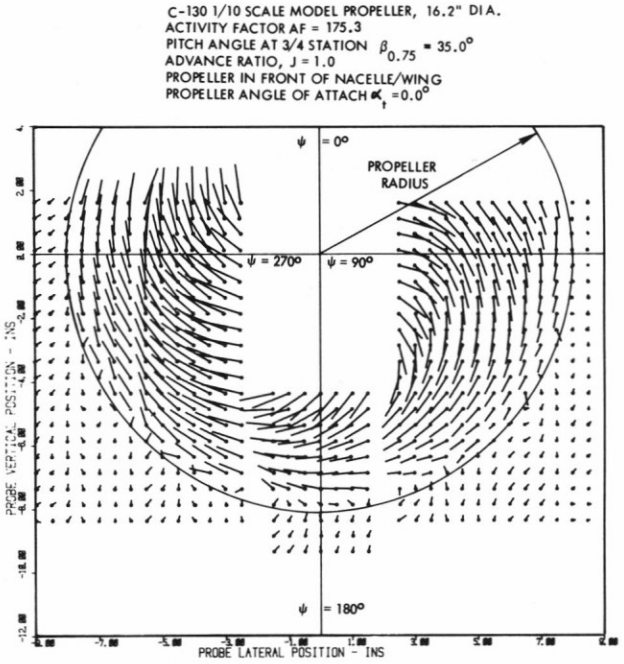

Figure 8. Vector Map of Wake Cross Flow (V-W Vectors)

The experimentally determined wake characteristics were compared with the calculations of the slipstream prediction program for the C-130 model propeller operating at an advance ratio of 1.0 and zero angle of attack. Figure 9 shows three curves of measured tangential induced velocity compared with a calculated curve. The tangential induced

velocity obtained from test data varies both with radius and azimuthal position because of nacelle/wing interference. Theory, on the other hand, assumes an isolated propeller with no azimuthal variation of tangential velocity. The theory best matches the $\psi = 180^{\circ}$ experimental curve, for which wing/nacelle interference is minimal. Wing/nacelle interference decreases tangential velocity along $\psi = 90^{\circ}$ and increases it along $\psi = 270^{\circ}$.

Figure 10 presents a comparison of measured and calculated swirl angle. As swirl angle is derived from tangential induced velocity, it also varies with azimuthal position in the experiment.

Measured Swirl Angles Followed Predicted Trends

It is also predicted that, for a propeller at angle of attack, the swirl angles in the horizontal axis of the propeller plane will increase along $\psi = 90^{\circ}$ and decrease along $\psi = 270^{\circ}$. This variation in swirl angle has two origins. The first is because the propeller is operating with an apparently varying advance ratio. This is predicted to cause a maximum difference of 9 percent in swirl angle at inboard blade stations and decreases toward the blade tip to about 4 percent. The second increment is due to the downward component of induced axial velocity. It is estimated that, for the present test, this will cause a maximum increment of 15 percent near the blade tip and will gradually decrease to about 5 percent at the 0.4 radial station. Thus, an average increase of about 14 percent in swirl angle is expected along $\psi = 90^{\circ}$ and a 14 percent reduction along $\psi = 270^{\circ}$. Figures 11 and 12 compare the experimental results at $\alpha = 0^{\circ}$ and $\alpha = 5^{\circ}$. It is seen that the difference in swirl angles is of the expected magnitude and sense.

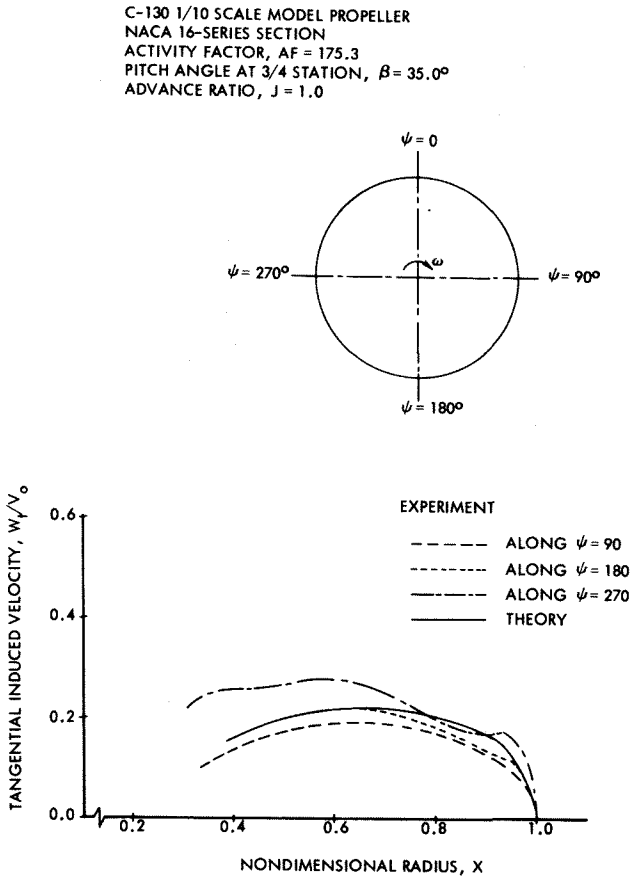

Figure 9. Comparison of Calculated and Measured Tangential Induced Velocity Distribution

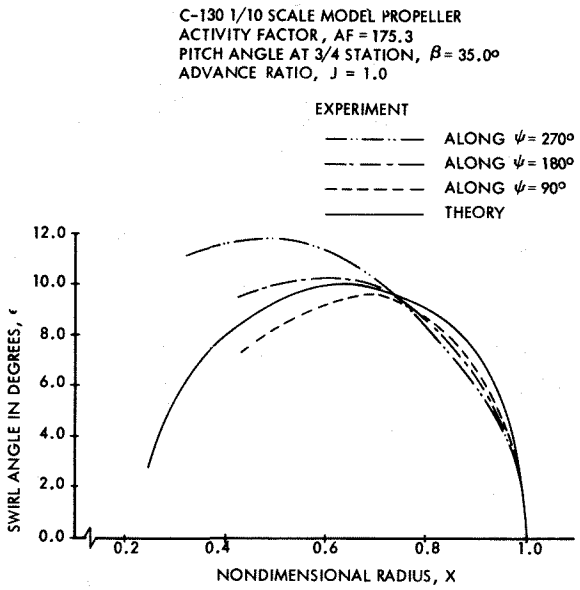

Figure 10. Comparison of Predicted and Measured Swirl Angles

The wing upwash indirectly affects the swirl angle by causing the propeller to experience an upward velocity along its plane, giving rise to sinusoidal variations of advance ratio with azimuthal position. This effect is the same as when the propeller is at an angle of attack. In addition, the upwash directly affects the nature of the wake by adding an upward velocity to it. These two effects are in opposition. The change in advance ratio increases swirl angle at $\psi = 90^{\circ}$ and reduces it at $\psi = 270^{\circ}$. The upward velocity on the slipstream decreases the swirl angle at $\psi = 90^{\circ}$ and increases it at $\psi = 270^{\circ}$. In most cases, the direct effect of the upwash is the stronger, because the magnitude of the wing-induced upwash increases as the distance forward of the wing leading edge is reduced. Figure 13 shows the effect of the wing upwash on swirl angles. As expected the swirl angle is slightly increased at $\psi = 270^{\circ}$.

Wing Behavior in A Propeller Slipstream

The propeller slipstream prediction program has been interfaced with the Aerodynamic Interference Program (AIP), which is a subsonic potential flow panel method currently in use at Lockheed for analysis of complex aerodynamic configurations. This program combination has been applied to a C-130 aircraft, and a typical configuration of the paneled aircraft is shown in Figure 14.

AIP is interfaced with the slipstream code by first identifying the wing panels which lie within the propeller slipstream. On these panels, the three-components of the impinging swirling flow are determined. These additional velocities are then simulated mathematically by a restatement of the

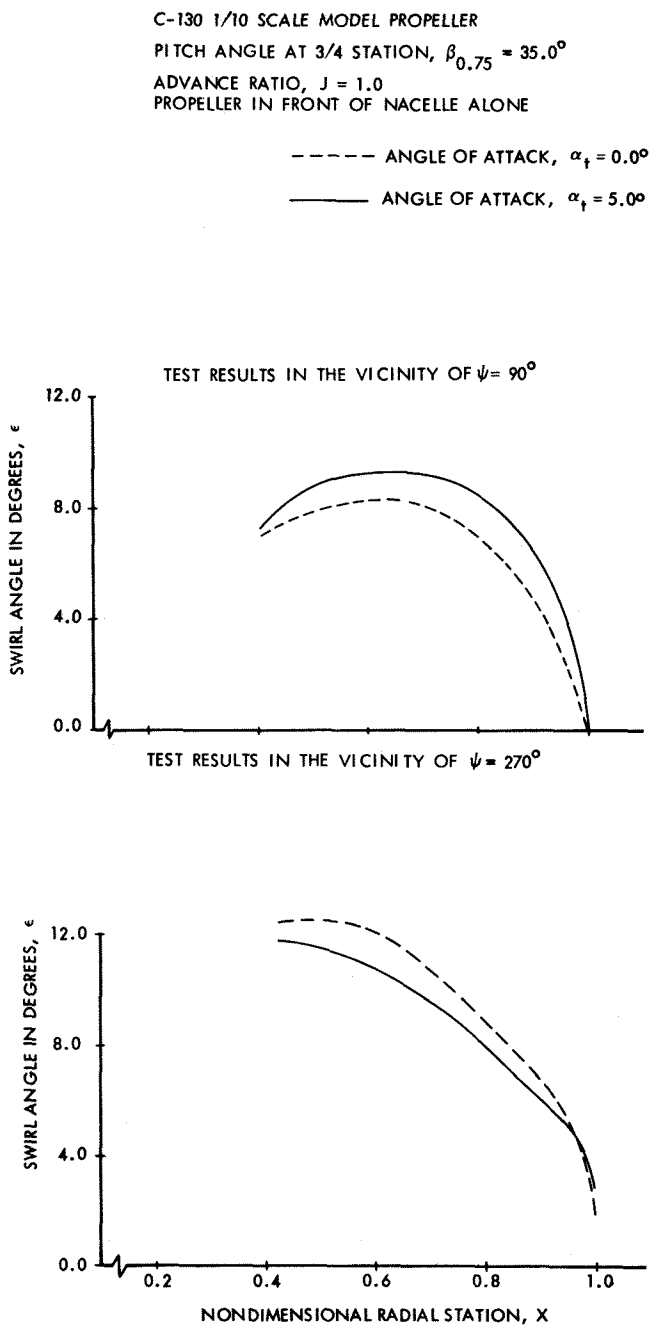

Figure 11. Effect of Thrust Axis Inclination on Swirl Angle

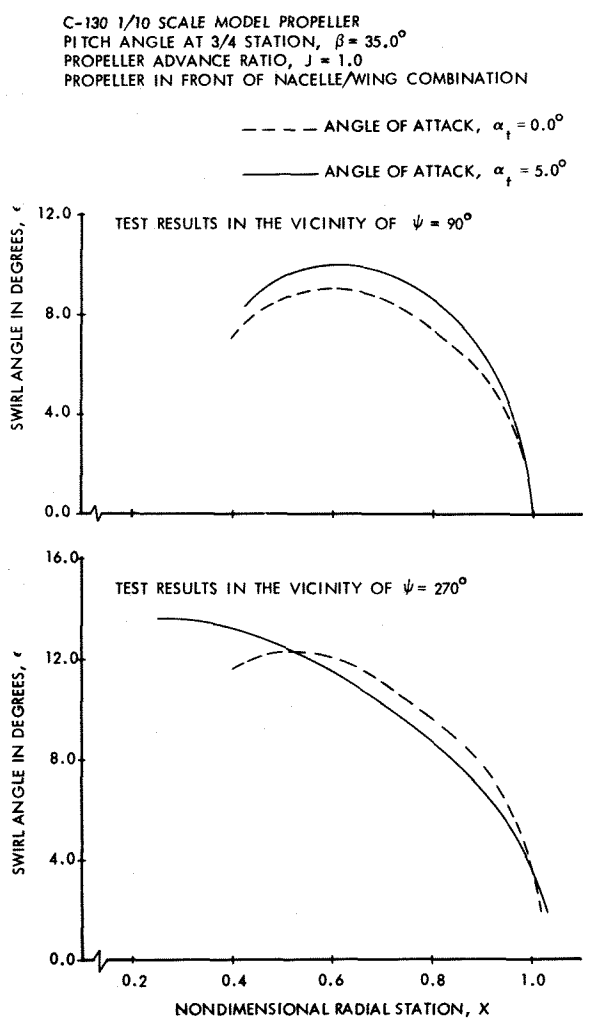

Figure 12. Effect of Thrust Axis Inclination on Swirl Angle

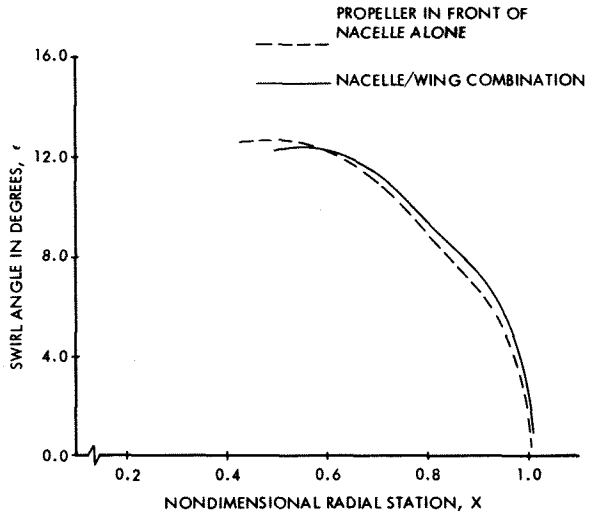

Figure 13. Effect of Wing Upwash on Swirl Angle

boundary conditions, so that the solution again satisfies the tangency requirement on all panel surfaces.

A comparison of the spanwise loading on the wing with and without propellers is shown in Figure 15. The effect of swirl is particularly evident on the inboard side of the propeller disc. Here it acts as an upwash, and the resulting increase in wing load is demonstrated.

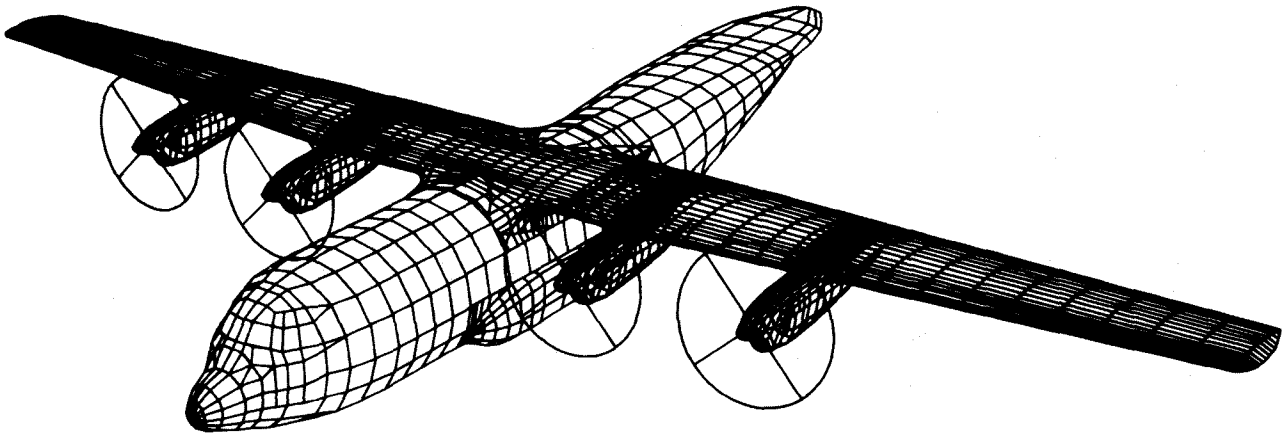

Figure 14. Paneling Scheme of C-130 Aircraft

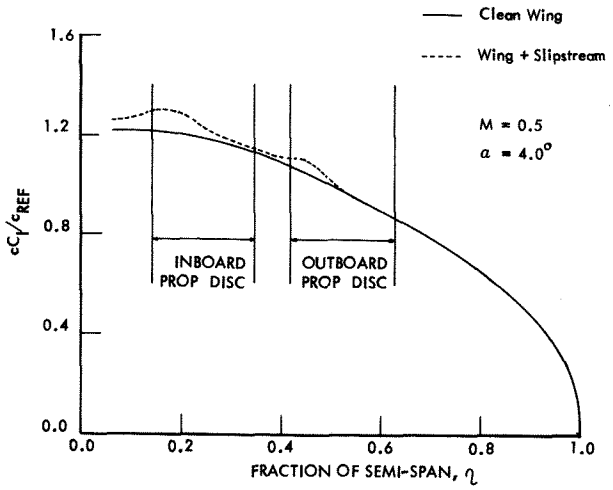

Figure 15. Effect of Slipstream on Span Loading

CONCLUDING REMARKS

1) The theory developed here provides a simple technique which predicts the aerodynamic properties of the propeller wake. The method is however dependent on accurate blade section aerodynamic data.

2) The presence of both the nacelle and wing affect the swirl angle induced by the propeller. The effect of the nacelle becomes more prominent at inboard blade stations. The wing effect tends to be small and depends on the particular configuration. The C-130 wing considered here caused a maximum increment in swirl angle of 5%.

3) The slipstream coupled with the potential flow model appears to adequately represent the pertinent features of a turboprop airplane, thus providing a means of evaluating the tradeoff available from relative arrangements of the propeller/nacelle/wing combination, in the subsonic regime.

4) The method developed here is strictly applicable to propellers with axisymmetric nacelles at zero angle of attack. Corrections need to be incorporated within the program to reflect azimuthal variation of slipstream properties due to thrust axis inclination or nacelle/wing presence.

References

1. Rohrback, Carl, "A Report on the Aerodynamic Design and Wing Tunnel Test of a Prop-Fan Model," AIAA Paper No. 76-667, July 1976.

2. Aljabri, A. S., "Prediction of Propeller Slipstream Characteristics," Lockheed Engineering Report LG79ER0120, October 1979.

3. McCormick, B. W., Jr., Aerodynamics of V/STOL Flight, Academic Press, New York, 1967.

4. Crigler, J. L., and Gilman, J., Jr., "Calculations of Aerodynamic Forces on a Propeller in Pitch or Yaw," NACA TN 2585, January 1952.